Investigation of material flow and thermomechanical behavior during friction stir welding of an AZ31B alloy for threaded and unthreaded pin geometries using computational solid mechanics simulation

R. A. R. Giorjao[1,2,*], E. B. Fonseca[3], J. A. Avila[4], E.F. Monlevade[1] and A.P. Tschiptschin[1].

[1]University of São Paulo, Metallurgical and Materials Engineering Department, Av. Prof. Mello Moraes 2463, 05508-030 São Paulo, SP, Brazil
[2]The Ohio State University, 1248 Arthur E. Adams Drive, Columbus, OH 43221, USA
[3]School of Mechanical Engineering, University of Campinas, Rua Mendeleyev 200, Campinas, SP 13083860, Brazil
[4]São Paulo State University, Campus of São João da Boa Vista, Av. Profa Isette Corrêa Fontão, 505, Jardim das Flores, 13876-750 São João da Boa Vista, SP, Brazil

*Corresponding author: R. A. R. Giorjao at The Ohio State University, e-mail address: rafael.arthur00@gmail.com

ABSTRACT

In the friction stir welding process, the tool role in the material flow and its thermomechanical behavior is still not entirely understood. Several modeling approaches attempted to explain the material and tool relationship, but to this date, insufficient results were provided in this matter. Regarding this issue and the urgent need for trustful friction stir welding models, a computational solid mechanic's model capable of simulating material flow and defect formation is presented. This model uses an Arbitrary Lagrangian-Eulerian code comparing a threaded and unthread pin profile. The model was able to reproduce the tool's torque, temperatures, and material flow along the entire process, including the underreported downward flow effect promoted by threaded pin's. A point tracking analysis revealed that threads increase the material velocity and strain rate to almost 30% compared to unthreaded conditions, promoting a temperature increment during the process, which improved the material flow and avoided filling defects. The presented results showed the model's capability to reproduce the defects observed in real welded joints, material thermomechanical characteristics and high sensitivity to welding parameters and tool geometries. Nevertheless, the outcomes of this work contribute to essential guidelines for future friction stir welding modeling and development, tool design, and defect prediction.

Keywords: computational solid mechanics; friction stir welding; material flow modeling; design of tools; light alloys; magnesium alloys

1. INTRODUCTION

Friction stir welding (FSW) is a solid-state technique in which severe plastic deformation and heat generation results in the processing and joining of similar and dissimilar materials. Features such as high-strength welds and small post-welding distortion made the FSW an excellent alternative for fusion welding, capable to also avoid its problems related to melting and solidification. Such a method has been applied to a wide range of materials in critical applications [1–5], promoting an aggressive need for optimization and development in friction stir welding scenarios.

During the process, the tool provides intense material deformation, which results in bonding between materials. The understanding of tool/processed material relationships during FSW is desirable for the process parameter optimization, microstructure control, and predictions of welded joint properties. It is well known that the tool used at FSW impacts the microstructures of welded joint and mechanical properties, but how it does it, is not fully comprehended [6]. Likewise, its effect on the flow of material is still one of the least understood phenomena due to the complexity and difficulty of visualization and measurement restrictions. Threaded tools have been considered efficient, avoiding the formation of defects, producing sound welds effectively by improving the material flow in aluminum alloys [7], and magnesium alloys [8].

Considered a fast and cost-reduction analysis, the numerical simulation of the FSW process analysis has become a powerful tool to support the real process. Nevertheless, the numerical modeling of the friction stir welding process has some challenges due to simultaneous high strain, strain rate, and temperature. Studies have been attempted to simulate temperature, strain, strain rate, and material flow in FSW in the past years [9–13]. Despite being fast and efficient methods for calculating temperatures of the friction welding process, computational fluid dynamics (CFD) models need to assign viscosity to the material and generally shows an over-prediction of the velocity fields and inability to predict defects generated by the process parameters and tool response to the process [14]. Kadian et al., [15] work considered different types of tool pin geometries and their effects on the material flow. The results showed that conical threaded tools provide higher temperatures than smooth conical tools, although they provided smaller velocities in the material. In most studies using CFD models, the material strain is based on fluid shear stresses. Furthermore, the fluid assumption enables us to calculate some critical process characteristics, such as tool torque, the mechanical response of the material, and defect prediction.

Computational solid mechanics (CSM) based methods otherwise consider that the welding material remains solid during the process and has been extensively used in research [16–24]. The force equilibrium equation based on continuum mechanics and the resulting partial derivative equations (PDE). Long et al. [17] presented a 3D thermal-mechanical coupled finite element model and investigated the tool tilt angle effect during friction stir welding. This model was able to predict the thermal-mechanical state variables during the welding and the post-welding morphology of the weld. Gao et al. [16] reported the downward spiral movement affected by the shoulder, whereas the lower material first moves in an upward spiral mode affected by the pin and then moves downward. Pashazadeh et al. [19], explored FSW experiments and numerical simulation for a pure copper alloy. The hardness and microstructure of a copper workpiece were investigated. The numerical results for hardness showed good agreement with recorded experimental data, suggesting the calculated deformation and temperatures were accurate. However, recent CSM-based simulations had not included threaded geometries due to extensive computational process-times and numerical robustness.

Due to the different results focused on individual issues, more studies including modeling from a holistic approach are needed to obtain information about the effect of tool geometries in material flow, thermomechanical behavior, and, consequently, defect prediction capabilities.

Here, based on the good results presented by CMS models, numerical simulation of the friction stir process using CSM-based DEFORM 3D software was explored. Pin geometry effects were evaluated using a new mesh approach to overcome the challenges related to large element distortion. Moreover, thermal-mechanical conditions of the material for the welding cases with and without threads are compared, the thread effects on strain rate, temperature, and flow paths were explained.

2. EXPERIMENTAL SETUP

2.1. Tool design and welding parameters

The FSW tool material was H13 steel with a 36-mm concave shoulder. The tool design was developed *in-house*. Figure 1 (a) shows the schematic and real pins' view, which considers the basic conical geometries with and without threads. The threaded type has a pitch of 3.5 mm, and the unthreaded is flat, without threads. The pins had a 7.5-mm diameter at the base and a total length of 8-mm.

Sheets of AZ31 magnesium alloy with the dimensions of 200mm x 50mm x 5 mm were used in lap position. Table 1 shows the FSW parameters employed in experimental and simulation approaches. The experimental welding temperatures were measured using K-type thermocouples placed 15 mm away from the weld center, 75 mm from the end of the plate and 2.5 mm depth from the top surface, on both sides, as shown in Figure 1 (b). The tool torque was monitored and recorded in real-time by the FSW machine spindle using the instantaneous power and current of

the motor. In Figure 1 (c), the weld schematic shows the maximum contact gap (20 mm) provided by the shoulder.

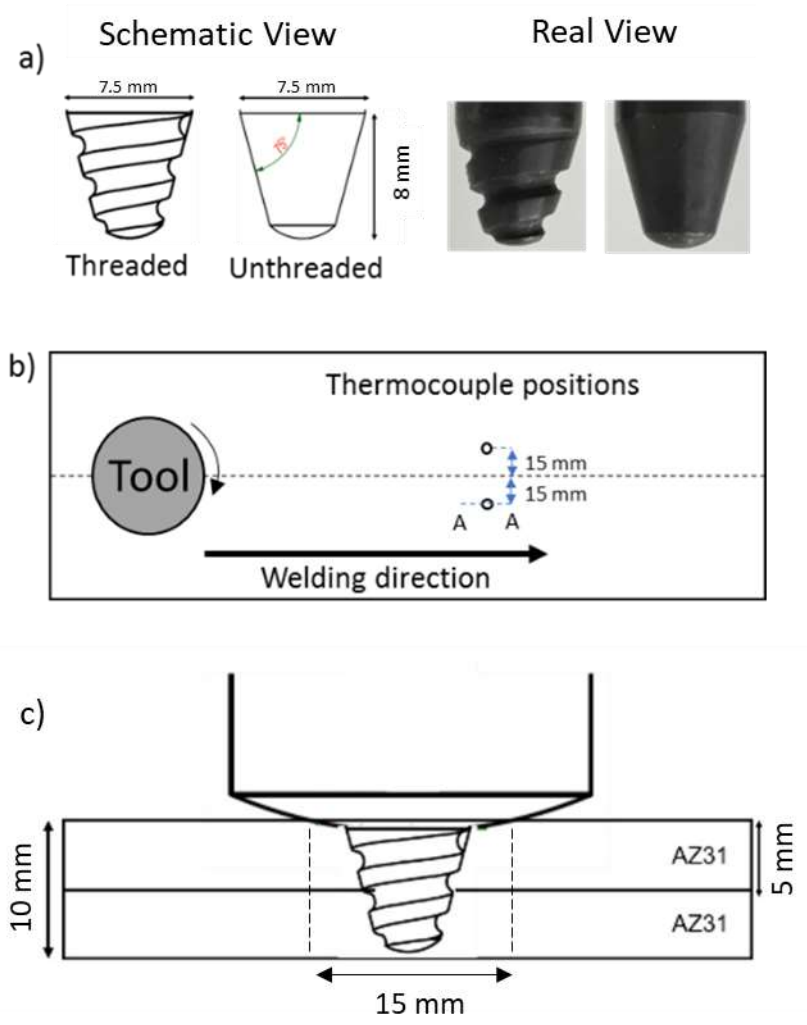

Figure 1: (a) Schematic and real view of the pins; (b) Thermocouple positions on the plate

Table 1: FSW parameters for the experimental tests and numerical simulation

Spindle Speed (RPM)	Traverse Speed (mm.min^{-1})	Pin Geometry	Short identification
800	200	Threaded	T82
	200	Unthreaded	U82

2.2. Material model

In order to simulate the material behavior during hot deformation, the material relationship between flow stress on temperature and strain rate was required. Empirical equations usually are applied to establish the deformation activation energy and hot deformation behavior of alloys. The Arrhenius relationship based on Sellars and McTegart [25] equations are one of the most frequently used, relating the strain rate, flow stress, and temperature. The selected parameters were acquired from an AZ31 hot deformation analysis performed by Giorjao et al., [26]. The temperatures (up to 500 ^{o}C), strain, and strain rate (up to 10 s^{-1}) range evaluated by the author fit well with the expected mechanical behavior observed in friction stir welding processes. A flow stress equation was obtained as shown in Equation 1,

where σ is the flow stress (MPa), $\dot{\varepsilon}$ is the applied strain-rate (s^{-1}), R is the gas constant and T is the temperature (K).

$$\dot{\varepsilon} = 4.79\, x\, 10^{9}\, [sinh(0.014\sigma)]^{3.88}\, e^{\left[\frac{-128000}{RT}\right]} \qquad \text{Equation 1}$$

2.3. Numerical modeling considerations

The simulations were performed using the finite element analysis software DEFORM-3D. This software can simultaneously perform material deformation, and thermal history using an Arbitrary Lagrangian-Eulerian (ALE) formulation. The arbitrary Lagrangian-Eulerian (ALE) is a finite element formulation in which the computational system is not a prior fixed in space (e.g., Eulerian-based finite element formulations – CFD models) or attached to the material. In the ALE method, the mesh nodes can move arbitrarily, bringing the freedom of the mesh movement and allowing significant distortions of the continuum. This feature alloys precise material distortion and deformation emulation (and also material flow defects - voids), which are the core events in the solid-state hot deformation process of friction stir welding.

The welding tool was assumed rigid and the workpiece as a rigid viscoplastic material. Additional details on governing equations can be found in the works of Buffa et al. [22,27] and Jain et al. [28]. The mesh workpiece was divided into two regions with different assignments, a deformable region located under the tool pin and shoulder, and an only-heat-transfer rigid region domain field. The thermal contact interaction between the two regions was considered perfect. The deformable region was designed with a 20 mm width. No significant alteration is expected beyond this distance in the base material. Thus, the mesh was refined locally (tool and workpiece contact area), and the simulation processing time optimized. The mesh schematics can be seen in Figure 2. The model considered one single plate instead of two stacked plates to reduce the contact interactions and save computational time.

The deformable region was meshed with about 60000 tetrahedral elements with a mean element size of 0.35 mm. The heat-transfer-only region was meshed with about 10000 elements. The tool was meshed with about 15000 tetrahedral elements. Figure 2 illustrates the contact area between the workpiece and tool, where the friction model was applied.

The heat transfer between the workpiece and ambient, and the tool and ambient was set equal to 20 W/m^{2}K, and the Heat transfer between the workpiece and tool was set equal to 22000 W/m^{2}K according to Asadi et al. [11]. The material flow was treated with an adaptive re-meshing finite element formulation.

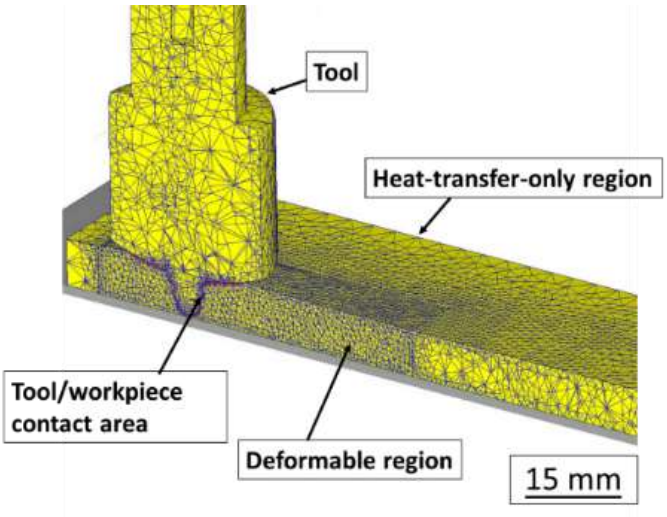

Figure 2: Mesh schematics indicating the tool domain, deformable and non-deformable regions, and the tool/workpiece area

2.4. Friction

In the FSW process, the friction coefficient is affected by temperature, pressure, among other variables, which makes it complex to determine its value. A trial-and-error method was adopted in this study due to the lack of experimental evidence of the high-temperature friction coefficient. To define the best friction coefficient, axial forces, and modeling temperatures, four different friction factors were calculated: 0.4, 0.6, 1, and 1.3, under 200 mm/min traverse speed and 800 rpm rotational speed. By comparing the simulated temperature results with the experimental ones, a good match was observed at the friction coefficient of 1.3.

Several authors have shown proper matching with experimental data using friction coefficient values below 1, e.g., 0.45 for Pashazadehet al. [19] and 0.3 for Gao et al. [16]. However, it is observed that all CSM models in literature explored only tools with small dimensions (below 6mm length) and simplified geometries [16–22]. In these cases, it is hypothesized that the selected low friction values are inaccurate; however, wrongly providing the right temperature according to calculations. These tools provide a simplified material flow that is easily achievable using low friction values. For large/complex tool geometries, the material movement tends to be more complicated as sticking/adhesion phenomena take a higher spot, which is achievable with low friction coefficients values.

Friction coefficient values above 1 are not very common in conventional metal forming processes. However, some studies sought to measure friction in typical conditions of friction stir welding such as pressure, tool geometry, and temperature. Duffin and Bahrani [29] determined that the friction coefficient can exceed the value of 1 by studying linear welding of steels. Similar results were found by Kumar et al. [30], who conducted experiments to study the interaction between the FSW tool and AA 7020-T6 sheets at various axial pressures and spindle speeds. The elevated contact pressures and temperatures experienced during the friction stir and similar processes promote a steep increase in the coefficient of friction identified to be due to the seizure phenomenon [31]. This phenomenon is observed when the contact condition between the rotating tool and the workpiece material changes from the slipping mode to a sticking/adhesion mode.

Figure 3 provides the tool surface covered with the AZ31B magnesium alloy. This result suggests that some of the processed material adhered to the tool surface, which supports the high friction values hypothesis during the friction stir processing.

Figure 3: Tools surface after the friction stir welding processing covered with the magnesium alloy

3. RESULTS AND DISCUSSION

3.1. Model validation

To verify the results obtained in the simulations, the temperature of the sheet and torque of tools from welding conditions T82 and U82, were exposed together, corresponding to the threaded and unthreaded tools with the spindle speed of 800 RPM and 200 mm/min, respectively.

The results in Figure 4 (a) and Figure 4 (b) showed proper matching with torque values for both conditions. Figure 4 (c) and Figure 4 (d) show the comparison between the thermal cycle of the experimental welding and simulated welding. The simulation agrees well with the thermal cycle of the experiment, for heating and cooling rates, and peak temperature. It was noticed an increase in torque for the threaded tool, maximum values of 60 N.m for T82, and 50 N.m for U82, which is related to a higher material resistance for intricated geometries than the smooth probe as mentioned by Jonckheere et al. [32].

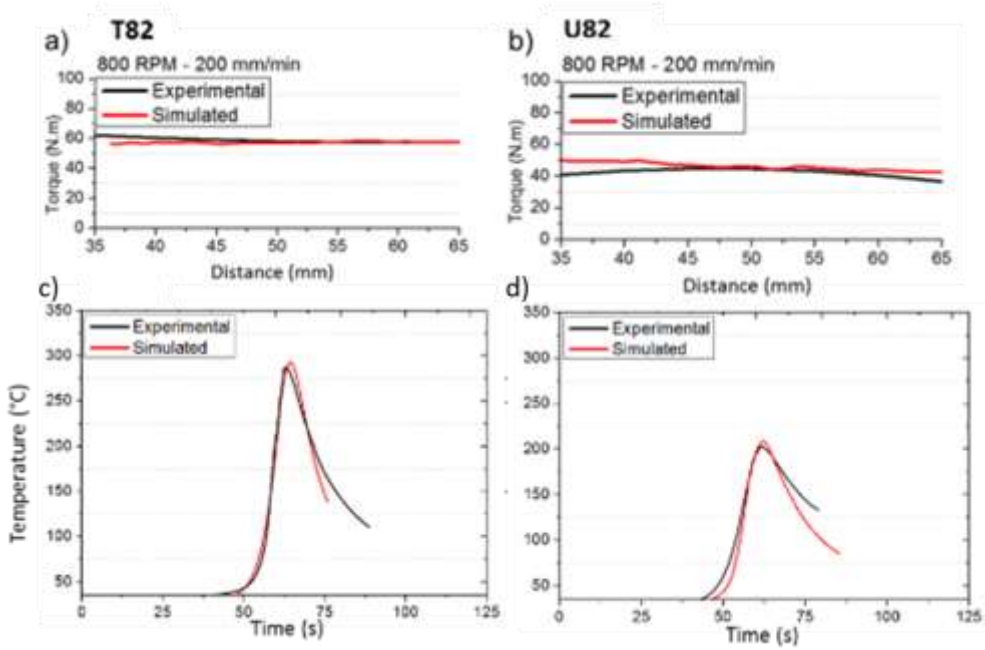

Figure 4: Comparison of tool torque values between simulation and experiment for (a) T82 condition and (b) U82 condition. Comparison of peak temperature between simulation and experiment at 15 mm far from the weld center and 2.5 mm depth from the surface for (c) T82 and (d) U82

3.2. Joint morphology

In the DEFORM software, the 3D slicing feature was used to observe internal features evolution along the cross-section of the weld. Experimental and simulated cross-sections joints were compared in Figure 5. As observed, the model successfully represented the experimental results, where even the defects position and approximately volume were calculated. It is possible to observe a significant void defect in the unthreaded condition. Even though there is a difference in the morphology of the defects, this numerical model could predict the tendency of defect production.

According to many related studies, void defects always occurred in the stir zone (SZ) on the advancing side (AS) and have a substantial relationship with the heat input generated by pin geometry and parameters, providing a lack of material flow and insufficient plastic deformation selected [33–37]. Failla [35] related void defect formation with the heat input applied to the weld. Increasing the linear travel speed reduced the heat input, which resulted in faster cooling of the material before this region becomes filled with stirred material. Toumpis et al. [36] stated that void defects in FSW of DH36 steel appear when the heat input from the tool is insufficient, and thus, a lack of material flow may occur. Rasti [37] performed an analytical study linking the heat input and void area for several welds in 1060 aluminum alloy. The author was able to identify a minimum heat input generation to create the tunnel void-free welds. The potential causes for the defects observed and simulated, such as temperatures and material deformation behavior, will be discussed in the following sections.

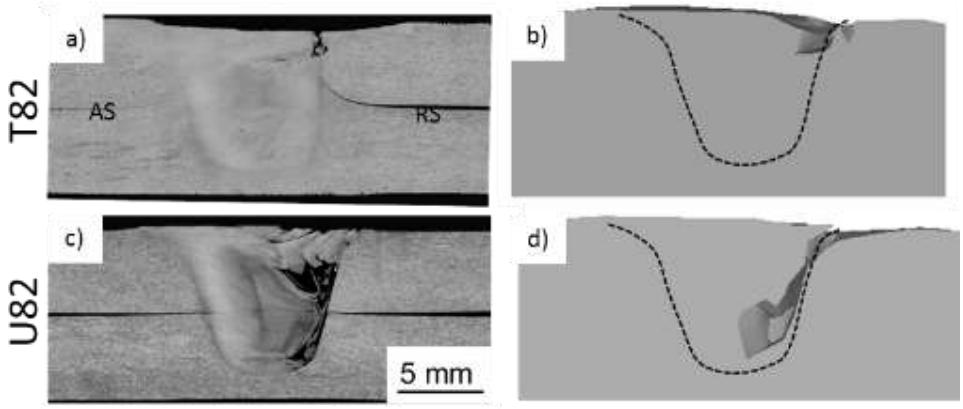

Figure 5: Experimental and simulated welded cross-sections for different welding parameters and pin geometries. Tools positions indicated in simulation for visualization proposes

3.3. Material thermomechanical history evaluation using a point tracking technique

For the material history evaluation, a point tracking technique was applied. The material behavior plays a critical role in determining the weld quality of FSW, which can be observed by the marker tracking method in the simulation results [38]. An arbitrary point was chosen at the center of the weld bead (X=0 mm) and a specified height (Z=7.25 mm) from the baseline for each condition, and its position, deformation, velocity, and temperature were evaluated, as seen in Figure 5.

In both conditions, observing the X curve, the movement around the tool is noted. Here, the simulations reveal that the material performs one semi-cycle around the tool, returning its initial transverse position. In the literature [17,39], similar flow behavior is also predicted by simulations and experimental observations.

However, the points presented different responses on vertical movement, as the threads provided an intense material downflow. It was calculated almost 4-mm vertical amplitude from maximum to the minimum height position in threaded condition. The downflow took almost 0.5 seconds. Then, the material returns to the initial vertical position. On unthreaded condition, a slight vertical movement was noted without the downward flow observed on the threaded tool. The material is retained in the weld bead by the tool shoulder action. Here we notice the difference of the trajectory imposed by the different pin geometries.

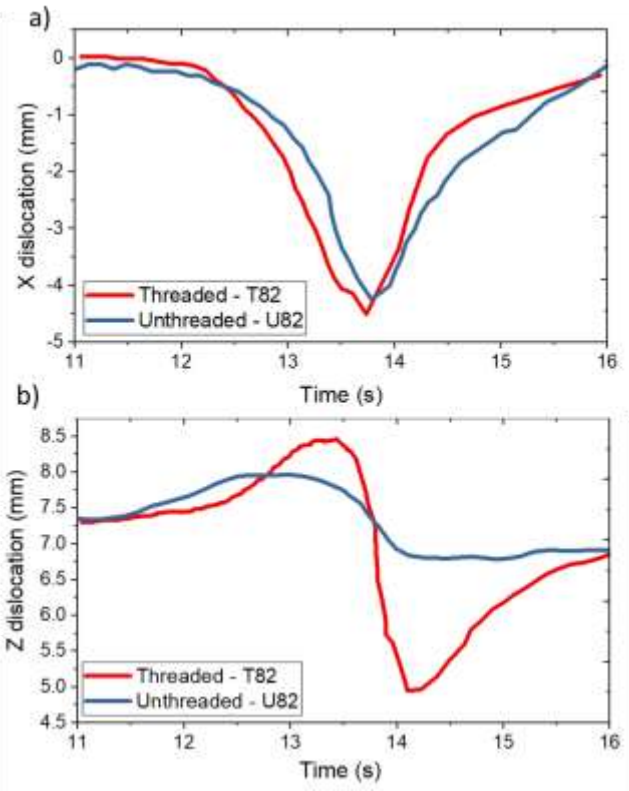

Figure 6: Comparison of the point position between the (a) threaded and (b) unthreaded condition

After evaluating point positions, the deformation and velocity on these points were analyzed. Figure 6 displays the points' velocity and strain rate during their processing. It was noticed that both velocity and strain rate have higher values in the threaded condition, reaching maximum values at the tool domain region (demarcated by dotted lines). Also, the peak velocity and strain rate values occur during the material downflow movement. In terms of velocity and strain-rate values, the threaded provides an almost 30% increase for the same rotation and welding speed.

Moreover, the overall values of strain rate and velocity are smaller and show less difference between threaded and unthreaded conditions than those found in the literature of CFD simulations. According to the velocity values, the maximum velocity observed was 15 $mm.s^{-1}$. Results found in the literature indicate higher values when performed in CFD, such as 3.43 $m.s^{-1}$ found by Kadian et al. [15], between 2 and 4 $m.s^{-1}$ by Ji et al. [40], indicating a difference in orders of magnitude from the present results. The higher values, as mentioned before, are due to the liquid assumptions for CFD models. CFD also showed higher values for strain-rate compared to the present work, for example, 500 s^{-1}, according to Chen et al. [41].

Through visualization of markers with X-rays, Morisada et al. [42] in aluminum welds at 1000 RPM estimate the material velocity and strain-rate during friction stir welding. The material's velocity varied in a range between 50-300 $mm.s^{-1}$, and the strain-rate reached a maximum of 15 s^{-1}, values similar to those found in the present work, and in similar works using the CSM approach [21,24]. It is valuable to mention that the presented fiction coefficient assumption did not provide unreliable strain-rate and velocity values for the material according to both experimental and similar models found in the literature [21,24,42].

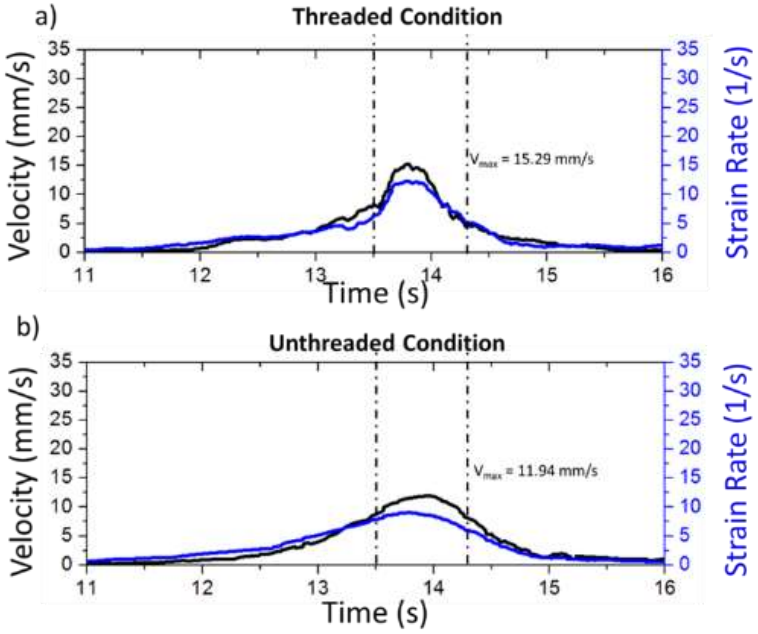

Figure 7: Comparison of the simulated point velocity and strain rate between (a) threaded and (b) unthreaded pins

The temperature profile for both points was also evaluated and is shown in Figure 7. The threaded condition presented higher values of temperature during welding, mostly during the tool domain region. The threaded condition point reached almost 500 °C, while the unthreaded point reached 425 °C. The same results are also presented in Figure 8, which shows a longitudinal cross-section and the calculated temperatures during processing. Its observed the higher temperatures are around the pin, and, higher values for the threaded condition.

The result was already expected due to the higher deformation velocities applied by tool threads. The peak temperature in threaded condition coincides with the downflow movement, maximum velocity, and maximum strain-rate values. Hence, the simulated values show the geometrical changes in the tool profile corresponds to almost 15% of the maximum temperature gain during material processing, using the same parameters.

In that way, tool threads provided an additional downflow movement, which comes with an additional increase in velocity and strain-rate. The increase in the deformation rate leads to a temperature increase during the process. A higher temperature and material velocity promote a higher capacity to the material to flow and fill the void generated by the tool during the process. Finally, as shown in the experimental welding trials, these effects combined lead to fewer defect formation probabilities.

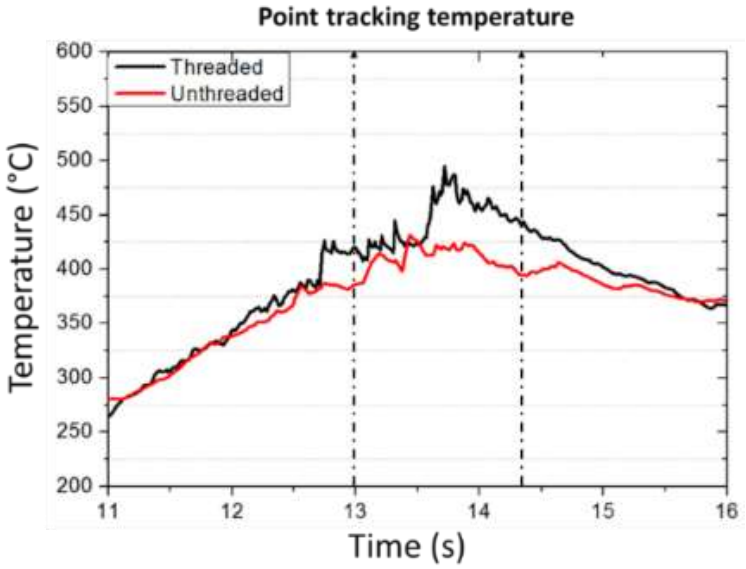

Figure 8: Simulated point tracking temperature profiles for threaded and unthreaded conditions

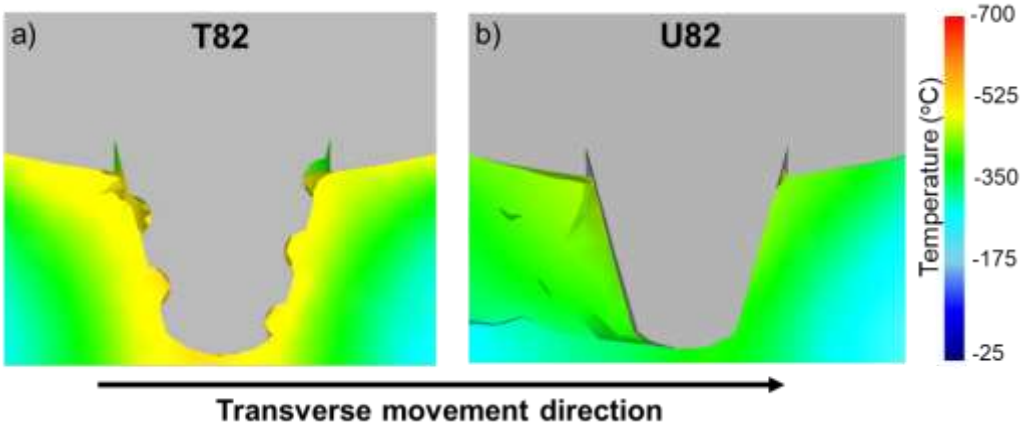

Figure 9: Longitudinal cross-section revealing the local temperatures during processing for the (a) threaded condition and (b) unthreaded condition

The microstructure of both conditions was compared to check if the temperature calculated by the model was consistent. Figure 10 (a) shows the microstructure for base metal condition, Figure 10 (b) for the T82 condition, and Figure 10 (c) for the U82 condition. Both processed microstructures show an equiaxed grain structure for the average grain size of 7.78 µm for T82 and 6.70 µm for U82. As observed, no critical microstructural difference occurred between the two conditions.

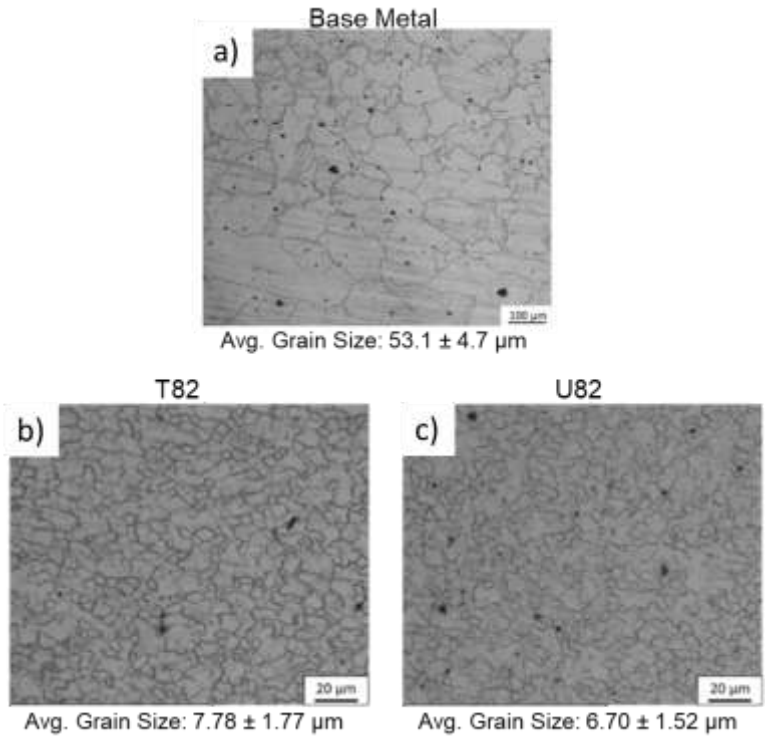

Figure 10: (a) Stir zone microstructure for T82; (b) Stir zone microstructure for U82

Finally, to verify the reliability of temperature and strain rate calculated by the model, the Zener-Holloman parameter (Z) was calculated using averages temperatures and strain-rate values provided by the present simulation and compare to hot deformation analysis in literature. The calculation results were compared to Maksoud et al., [43] work, where the author delivered a Zenner-Holloman (Z) and dynamic recrystallized grain size relationship for the AZ31 magnesium alloy. According to results in Figure 11, the temperature and deformation behavior calculated by the model provided similar values of grain sizes from those measured in Figure 10, which suggests accuracy on the present model assumptions and results.

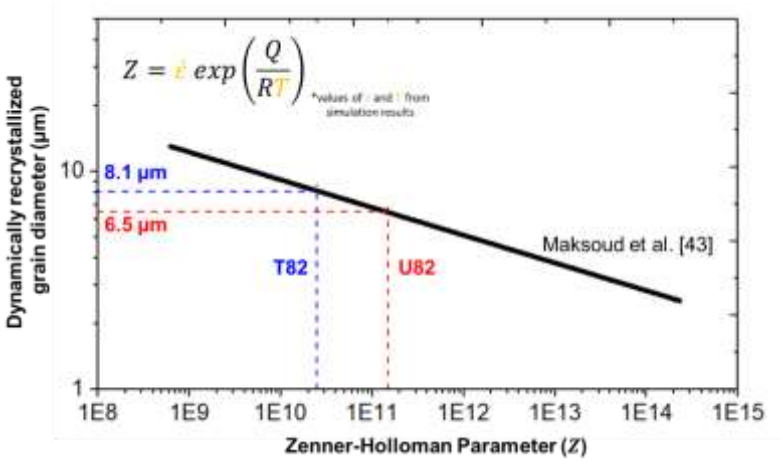

Figure 11: Calculated Zenner-Holloman parameters and expected recrystallized grain diameters

4. Conclusions

In this research work, friction stir welding of AZ31B Magnesium alloy was successfully simulated using the DEFORM-3D software. The simulation could calculate temperature, tool response, cross-section geometry, strain, strain rate, and material flow. Regarding the methodology and presented results, some conclusions are presented:

- The simulation indicates that pin with threads provided a material downward flow. The additional movement and deformation offered by threads increased the temperature of the material for the same welding parameters.
- The peak temperature in the threaded condition coincides with the point of downward flow, maximum velocity, and maximum strain rate values. On the other hand, the unthreaded tool generated a slight vertical movement without a significant downward flow.
- Calculated values of velocity and strain-rate show much lower values compared to widely employed CFD simulations. However, the present results are equivalent to the experimental results found in the literature. These results also support the friction coefficient assumption taken on the present work.
- Zener-Holloman parameters calculated using calculated values of deformation rate and temperature shows the consistency of the values presented by the model.

5. Acknowledgments

The authors acknowledge the financial support provided by the Brazilian Nanotechnology National Laboratory (LNNano) of the Brazilian Center for Research in Energy and Materials (CNPEM) and Villares Metals.

6. References

[1] H. Shirazi, S. Kheirandish, M.A. Safarkhanian, Effect of process parameters on the macrostructure and defect formation in friction stir lap welding of AA5456 aluminum alloy, Measurement. 76 (2015) 62–69. https://doi.org/10.1016/j.measurement.2015.08.001.

[2] J.A. Avila, J.F. Rodriguez, P.R. Mei, A.J. Ramirez, Microstructure and fracture toughness of multipass friction stir welded joints of API-5L-X80 steel plates, Mater. Sci. Eng. A. 673 (2016) 257–265. https://doi.org/10.1016/j.msea.2016.07.045.

[3] J.A.D. Ávila, E. Lucon, J.W. Sowards, P.R. Mei, A.J. Ramirez, Ductile-to-Brittle temperature transition curve assessment of the stirred, hardest and heat affected zones within a FSW joint of API 5L X80 steel by testing miniaturized Charpy V-notch specimens, Metall. Mater. Trans. A. Submitting (2015) 1–22.

[4] Z.Y. Ma, A.H. Feng, D.L. Chen, J. Shen, Recent Advances in Friction Stir Welding/Processing of Aluminum Alloys: Microstructural Evolution and Mechanical Properties, Crit. Rev. Solid State Mater. Sci. 43 (2018) 269–333. https://doi.org/10.1080/10408436.2017.1358145.

[5] E.. Mubiayi, M.P & Akinlabi, Friction Stir Welding of Dissimilar Materials : An Overview, Int. J. Mech. Aerospace, Ind. Mechatronics Eng. 7 (2013) 240–245. https://doi.org/10.1016/B978-0-12-802418-8.00005-9.

[6] R. Rai, H.K.D.H. Bhadeshia, T. Debroy, Review : friction stir welding tools, Sci. Technol. Weld. Join. 16 (2011) 325–342. https://doi.org/10.1179/1362171811Y.0000000023.

[7] M. Reza-E-Rabby, A.P. Reynolds, Effect of Tool Pin Thread Forms on Friction Stir Weldability of Different Aluminum Alloys, Procedia Eng. 90 (2014) 637–642. https://doi.org/10.1016/j.proeng.2014.11.784.

[8] G. Padmanaban, V. Balasubramanian, Selection of FSW tool pin profile, shoulder diameter and material for joining AZ31B magnesium alloy – An experimental approach, Mater. Des. 30 (2009) 2647–2656. https://doi.org/10.1016/j.matdes.2008.10.021.

[9] L. Fratini, G. Buffa, D. Palmeri, J. Hua, R. Shivpuri, Material flow in FSW of AA7075–T6 butt joints: numerical simulations and experimental verifications, Sci. Technol. Weld. Join. 11 (2006) 412–421. https://doi.org/10.1179/174329306X113271.
[10] G. Buffa, A. Ducato, L. Fratini, Numerical procedure for residual stresses prediction in friction stir welding, Finite Elem. Anal. Des. 47 (2011) 470–476. https://doi.org/10.1016/j.finel.2010.12.018.
[11] P. Asadi, R.A. Mahdavinejad, S. Tutunchilar, Simulation and experimental investigation of FSP of AZ91 magnesium alloy, Mater. Sci. Eng. A. 528 (2011) 6469–6477. https://doi.org/10.1016/j.msea.2011.05.035.
[12] P. Asadi, M.K. Besharati Givi, M. Akbari, Simulation of dynamic recrystallization process during friction stir welding of AZ91 magnesium alloy, Int. J. Adv. Manuf. Technol. 83 (2016) 301–311. https://doi.org/10.1007/s00170-015-7595-z.
[13] A.F. Hasan, CFD modelling of friction stir welding (FSW) process of AZ31 magnesium alloy using volume of fluid method, J. Mater. Res. Technol. 8 (2019) 1819–1827. https://doi.org/10.1016/j.jmrt.2018.11.016.
[14] P. a. Colegrove, H.R. Shercliff, 3-Dimensional CFD modelling of flow round a threaded friction stir welding tool profile, J. Mater. Process. Technol. 169 (2005) 320–327. https://doi.org/10.1016/j.jmatprotec.2005.03.015.
[15] A.K. Kadian, P. Biswas, Effect of tool pin profile on the material flow characteristics of AA6061, J. Manuf. Process. 26 (2017) 382–392. https://doi.org/10.1016/j.jmapro.2017.03.005.
[16] E. zhi GAO, X. xing ZHANG, C. zhong LIU, Z. yi MA, Numerical simulations on material flow behaviors in whole process of friction stir welding, Trans. Nonferrous Met. Soc. China (English Ed. 28 (2018) 2324–2334. https://doi.org/10.1016/S1003-6326(18)64877-0.
[17] L. Long, G. Chen, S. Zhang, T. Liu, Q. Shi, Finite-element analysis of the tool tilt angle effect on the formation of friction stir welds, J. Manuf. Process. 30 (2017) 562–569. https://doi.org/10.1016/j.jmapro.2017.10.023.
[18] N. Dialami, M. Cervera, M. Chiumenti, C. Agelet de Saracibar, A fast and accurate two-stage strategy to evaluate the effect of the pin tool profile on metal flow, torque and forces in friction stir welding, Int. J. Mech. Sci. 122 (2017) 215–227. https://doi.org/10.1016/j.ijmecsci.2016.12.016.
[19] H. Pashazadeh, A. Masoumi, J. Teimournezhad, Numerical modelling for the hardness evaluation of friction stir welded copper metals, Mater. Des. 49 (2013) 913–921. https://doi.org/10.1016/j.matdes.2013.02.058.
[20] H. Pashazadeh, J. Teimournezhad, a Masoumi, Numerical investigation on the mechanical, thermal, metallurgical and material flow characteristics in friction stir welding of copper sheets with experimental verification, Mater. Des. 55 (2014) 619–632. https://doi.org/10.1016/j.matdes.2013.09.028.
[21] H. Pashazadeh, A. Masoumi, J. Teimournezhad, A study on material flow pattern in friction stir welding using finite element method, Proc. Inst. Mech. Eng. Part B J. Eng. Manuf. 227 (2013) 1453–1466. https://doi.org/10.1177/0954405413485952.
[22] G. Buffa, J. Hua, R. Shivpuri, L. Fratini, A continuum based fem model for friction stir welding—model development, Mater. Sci. Eng. A. 419 (2006) 389–396. https://doi.org/10.1016/j.msea.2005.09.040.
[23] P. Asadi, M. Akbari, H. Karimi-Nemch, Simulation of friction stir welding and processing, in: Adv. Frict. Weld. Process., Elsevier, 2014: pp. 499–542. https://doi.org/10.1533/9780857094551.499.
[24] S. Tutunchilar, M. Haghpanahi, M.K.B. Givi, P. Asadi, P. Bahemmat, Simulation of material flow in friction stir processing of a cast Al – Si alloy, J. Mater. 40 (2012) 415–426. https://doi.org/10.1016/j.matdes.2012.04.001.
[25] C.M. Sellars, W.J. McTegart, On the mechanism of hot deformation, Acta Metall. 14 (1966) 1136–1138. https://doi.org/10.1016/0001-6160(66)90207-0.
[26] R.A.R. Giorjao, E.F. Monlevade, J.A. Avila, A.P. Tschiptschin, Numerical modeling of flow stress and grain evolution of an Mg AZ31B alloy based on hot compression tests, J.

Brazilian Soc. Mech. Sci. Eng. 42 (2020) 57. https://doi.org/10.1007/s40430-019-2146-4.
[27] G. Buffa, L. Fratini, Friction stir welding of steels: process design through continuum based FEM model, Sci. Technol. Weld. Join. 14 (2009) 239–246. https://doi.org/10.1179/136217109X421328.
[28] R. Jain, S.K. Pal, S.B. Singh, Thermomechanical Simulation of Friction Stir Welding Process Using Lagrangian Method, in: Simulations Des. Manuf., Springer Singapore, 2018: pp. 103–146. https://doi.org/10.1007/978-981-10-8518-5.
[29] F.D. Duffin, A.S. Bahrani, Frictional behaviour in friction welding of mild steel, 26 (1973) 53–74.
[30] K. Kumar, C. Kalyan, S. V. Kailas, T.S. Srivatsan, An investigation of friction during friction stir welding of metallic materials, Mater. Manuf. Process. 24 (2009) 438–445. https://doi.org/10.1080/10426910802714340.
[31] M. Mosleh, N. Saka, N.P. Suh, A mechanism of high friction in dry sliding bearings, Wear. 252 (2002) 1–8. https://doi.org/10.1016/S0043-1648(01)00583-X.
[32] C. Jonckheere, B. De Meester, A. Denquin, A. Simar, Torque, temperature and hardening precipitation evolution in dissimilar friction stir welds between 6061-T6 and 2014-T6 aluminum alloys, J. Mater. Process. Technol. 213 (2013) 826–837. https://doi.org/10.1016/j.jmatprotec.2013.01.001.
[33] P. Gulati, D.K. Shukla, A. Gupta, Defect formation analysis of Friction Stir welded Magnesium AZ31B alloy, Mater. Today Proc. 4 (2017) 1005–1012. https://doi.org/10.1016/j.matpr.2017.01.113.
[34] A. Gupta, P. Singh, P. Gulati, D. Kumar, Effect of Tool rotation speed and feed rate on the formation of tunnel defect in Friction Stir Processing of AZ31 Magnesium alloy, Mater. Today Proc. 2 (2015) 3463–3470. https://doi.org/10.1016/j.matpr.2015.07.322.
[35] D.M. Failla, Friction stir welding and microstructure simulation of HSLA-65 and austenitic stainless steels, The Ohio State University, 2009.
[36] C. Tingey, A. Galloway, A. Toumpis, S. Cater, Effect of tool centreline deviation on the mechanical properties of friction stir welded DH36 steel, Mater. Des. 65 (2015) 896–906. https://doi.org/10.1016/j.matdes.2014.10.017.
[37] J. Rasti, Study of the welding parameters effect on the tunnel void area during friction stir welding of 1060 aluminum alloy, (2018) 2221–2230.
[38] N. Dialami, M. Chiumenti, M. Cervera, C. Agelet de Saracibar, J.P. Ponthot, Material flow visualization in friction stir welding via particle tracing, Int. J. Mater. Form. 8 (2015) 167–181. https://doi.org/10.1007/s12289-013-1157-4.
[39] B.C. Liechty, B.W. Webb, The use of plasticine as an analog to explore material flow in friction stir welding, J. Mater. Process. Technol. 184 (2007) 240–250. https://doi.org/10.1016/j.jmatprotec.2006.10.049.
[40] S.D. Ji, Q.Y. Shi, L.G. Zhang, A.L. Zou, S.S. Gao, L. V. Zan, Numerical simulation of material flow behavior of friction stir welding influenced by rotational tool geometry, Comput. Mater. Sci. 63 (2012) 218–226. https://doi.org/10.1016/j.commatsci.2012.06.001.
[41] G. Chen, H. Li, G. Wang, Z. Guo, S. Zhang, Q. Dai, X. Wang, G. Zhang, Q. Shi, Effects of pin thread on the in-process material flow behavior during friction stir welding: A computational fluid dynamics study, Int. J. Mach. Tools Manuf. 124 (2018) 12–21. https://doi.org/10.1016/j.ijmachtools.2017.09.002.
[42] Y. Morisada, T. Imaizumi, H. Fujii, Determination of strain rate in Friction Stir Welding by three-dimensional visualization of material flow using X-ray radiography, Scr. Mater. 106 (2015) 57–60. https://doi.org/10.1016/j.scriptamat.2015.05.006.
[43] I.A. Maksoud, H. Ahmed, J. Rödel, Investigation of the effect of strain rate and temperature on the deformability and microstructure evolution of AZ31 magnesium alloy, Mater. Sci. Eng. A. 504 (2009) 40–48. https://doi.org/10.1016/j.msea.2008.10.033.